Journal of Engineering Geology and Environmental Research, Volume 2, 2026. pp 10 - 24

ISSN: 2992-5657
Available on: **www.naege.org/jeger**

Flood Prediction and Hazard Mapping Using QGIS and HEC-RAS for the Lower Niger River at Lokoja, Nigeria

Ahawike, J.K., [1]Akanmu, J.O.[1] and Inyang, M.M.[2*]

Abstract
Flooding is one of the deadliest climate hazard faced in Nigeria and recent times flood frequency and intensity has increased drastically. Lower Niger River at Lokoja-Kogi State tends to experience flood due to its location at the confluence of Niger and Benue Rivers. This research combined QGIS and HEC-RAS analysis to forecast the characteristics and spatial delineation of flood hazard zones using the hydrological data spanning 1995-2020. The Flood frequency analysis was conducted using Gumbel Extreme Value Distribution and the Return periods of 5, 10, 20, 30, 50, 100, 200 and 300 years were estimated. The corresponding peak discharges were 24,325 m^3/s, 27,184 m^3/s, 29,926 m^3/s, 31,504 m^3/s, 33,476 m^3/s, 36,137 m^3/s, 38,787 m^3/s, and 40,335 m^3/s, with associated water levels of 10.8 m, 11.6 m, 12.4 m, 12.7 m, 13.5 m, 14.3 m, 15.0 m, and 15.5 m, respectively. The model was calibrated with the 2012 flood and the simulated water level of 12.59 m compared closely with the observed level of 12.8 m. Simulation of the flood hazard assessment shows that with an increase in the return period there is a gradual increase in the discharge and flood extent as well. When compared to the historic flood event of 2012 (31,692 m^3/s; 12.8 m) there is roughly a 14% increase in discharge for the 100-year return period and more than a 27% increase for the 300-year return period. In conclusion, the combination of QGIS and HEC-RAS offers an effective data-driven methodology for flood prediction and hazard mapping to inform better flood risk management, spatial planning, and climate adaptation strategies in the Lower Niger Basin.

Keywords: *Flood prediction, Flood hazard mapping, Lower Niger River, HEC-RAS, QGIS, Gumbel Extreme Value Distribution*

Introduction

Flooding remains one of the most destructive environmental hazards globally because of its far-reaching effects on human life, infrastructure, agriculture, public health, and regional economies. In riverine environments, floods occur when water volumes exceed channel capacity and spill onto adjoining floodplains, submerging lands that are ordinarily dry (Emmanuel *et al.*, 2015; Rincón *et al.*, 2018). Such events are particularly severe in large river basins where dense populations, critical infrastructure, and agricultural activities concentrate along low-lying alluvial corridors. As emphasized by Afzal *et al.* (2022), floods are catastrophic natural hazards with major implications for both mortality and economic stability, while Santos *et al.* (2019) similarly noted that river flooding is a recurrent global disaster associated with extensive material and human losses. Beyond natural hydrometeorological controls, floods may also be intensified by hydraulic infrastructure failure or sudden water releases from dams. The 2012 inundation across much of the Lower Niger-Benue system in Nigeria, widely linked to release from the Lagdo Dam in Cameroon, remains an important historical reminder of the scale of devastation that can be produced when extreme river discharge interacts with highly exposed floodplain communities.

The growing urgency of flood studies is further reinforced by the changing hydroclimatic regime now observed in many parts of the world. Climate change is increasing the frequency, magnitude, and uncertainty of extreme hydrological events, thereby complicating prediction and intensifying the vulnerability of already exposed populations (IPCC, 2021; Korah & Cobbinah, 2019). In many African basins, however, flood-risk studies still tend to treat river systems as though they were spatially uniform, often overlooking the social, environmental, and geomorphic heterogeneities that influence flood generation, routing, inundation depth, and impact severity (Gaisie & Brandful, 2023; Ramayanti *et al.*, 2022). This limitation becomes especially critical in large convergent drainage systems such as the Lower Niger Basin, where interactions among upstream inflow, channel morphology, floodplain storage, settlement patterns, and land-use conversion can produce highly variable flood behaviour across relatively short distances. For environmental planning and public safety, therefore, reliable estimates of flood timing, magnitude, depth, and extent are indispensable for early warning, land-use regulation, infrastructure protection, and disaster-response planning.

✉ michaelm.inyang@gmail.com
1 Department of Civil and Environmental Engineering, University of Lagos, Lagos, Nigeria
2 Department of Geology, University of Port Harcourt, Choba, Port Harcourt, Nigeria

Published: August, 2026.

Flood modelling provides the principal analytical framework through which these processes can be understood and translated into actionable hazard information. In general terms, flood models are mathematical representations of hydrologic and hydraulic processes designed to reproduce the temporal and spatial behaviour of floodwaters and the hazards associated with them (Nikoo *et al.*, 2016; Gori *et al.*, 2019). These models support a wide range of applications, including flood forecasting, flood-risk assessment, mitigation planning, and emergency management (Wu *et al.*, 2019; Psomiadis *et al.*, 2021). Hydrologic models are commonly used to transform rainfall inputs into runoff responses, thereby estimating how much water enters a river system and when that contribution occurs within a catchment (Herrera *et al.*, 2022; Duchan *et al.*, 2022). Hydraulic models, by contrast, simulate the movement, storage, and stage behaviour of water within channels and floodplains as controlled by channel geometry, roughness, slope, and boundary conditions. Depending on study objectives, modelling frameworks may be continuous, for analysing long-term hydrological variability, or event-based, for reproducing specific extreme events and their consequences (Filipova *et al.*, 2019; Winter *et al.*, 2019).

Model dimensionality is another important consideration in flood studies. One-dimensional (1D) models are computationally efficient and remain widely used for channel-flow simulation; however, they often simplify lateral exchanges and may not adequately represent the complex hydraulics of floodplain inundation. Two-dimensional (2D) approaches are generally more suitable where the objective is to depict the spread of water both along and across floodplains, even though they demand greater computational effort and more detailed data inputs (Pinos *et al.*, 2019; Hankin *et al.*, 2019). Yet regardless of the modelling approach adopted, flood prediction is often constrained by uncertainty arising from incomplete or inaccurate hydrological, meteorological, topographic, and land-use data (Mondal *et al.*, 2023). In response, recent studies have increasingly incorporated advanced uncertainty-handling techniques such as Bayesian inference, Monte Carlo simulation, and optimization algorithms to improve model calibration and performance under data-limited conditions (Bauer-Marschallinger *et al.*, 2022; Clare *et al.*, 2022; Diao *et al.*, 2022). These advances have significantly enhanced the robustness of modern flood assessment, but they do not eliminate the need for reliable spatial datasets and a strong geospatial framework for model implementation.

In this regard, the integration of remote sensing, Geographic Information Systems (GIS), and hydraulic modelling has become one of the most effective approaches for contemporary flood analysis. GIS and remote-sensing datasets enable rapid extraction, processing, and visualization of terrain, land-cover, drainage, and inundation information, thereby improving both model setup and hazard interpretation (Schumann *et al.*, 2018; Nharo *et al.*, 2019). Compared with conventional field-based delineation methods, these techniques allow faster, broader, and often more accurate flood-extent estimation, particularly over large or logistically difficult terrains (Grežo *et al.*, 2020). Flood hazard maps derived from such integrated workflows provide critical decision-support tools for identifying zones susceptible to inundation and for guiding planning related to settlement control, infrastructure placement, insurance evaluation, and disaster-risk reduction (Chen *et al.*, 2022; Liu *et al.*, 2021). Within this broader methodological context, QGIS offers a flexible geospatial platform for terrain processing, spatial data integration, and map production, while HEC-RAS provides a widely accepted hydraulic modelling environment for simulating water-surface profiles and floodplain inundation under defined discharge scenarios.

The Lower Niger River Basin presents a compelling setting for the application of these tools because of its strategic downstream location, low-lying floodplain characteristics, and growing anthropogenic pressure. Urban expansion, agricultural development, and other land-surface modifications within the basin have progressively increased runoff generation and reduced infiltration, thereby exacerbating flood susceptibility in communities located near active river channels and flood-prone lowlands. Nigeria's recent flood history illustrates the seriousness of this problem. Although flooding is a recurrent phenomenon across the country, the 2022 flood disaster was widely regarded as the most severe since the 2012 event (Maclean, 2022). Reports indicate that more than two million people were affected during the 2022 floods (Akbarzai *et al.*, 2022), while fatalities exceeded 600 and injuries surpassed 2,400 by October of that year (Maclean, 2022); earlier reports had already documented 372 deaths by August (Matthew, 2022; Davies, 2022). Public-health consequences were also severe, including flood-related contamination of water sources and a cholera outbreak in northeastern Nigeria that caused at least 64 deaths (Davies, 2022). In addition, over 200,000 houses were reportedly destroyed or damaged, and approximately 110,000 hectares of agricultural land were devastated (Adetayo, 2022). The broader humanitarian implications were equally alarming: according to the United Nations system, the flooding significantly worsened food insecurity, with about 19 million people affected and 14.7 million children placed at risk of malnutrition, including large numbers vulnerable to severe acute malnutrition in northern and northwestern states (UN, 2022). These figures underscore the national importance of flood-risk assessment and the need for scientifically defensible prediction tools for areas influenced by the Niger River system.

Despite the frequency and severity of flood disasters in Nigeria, scientific and engineering information on inundation extent and return-period behaviour for the Lower Niger River remains insufficient for proactive planning. Many vulnerable populations continue to reside on floodplains and often return to the same locations after floodwaters recede, thereby sustaining a cycle of repeated exposure and loss. The lack of dependable local-scale flood prediction and hazard mapping has therefore remained a critical gap for communities, institutions, and decision-makers concerned with risk reduction and resilience building. It is against this background that the present study applies QGIS and HEC-RAS to predict flood behaviour and delineate hazard zones along the Lower Niger River. Specifically, the study processes and analyses relevant geospatial datasets within QGIS, applies the Gumbel Extreme Value Distribution to estimate flood magnitudes for return periods ranging from 5 to 300 years, simulates the corresponding flood extents in HEC-RAS, and compares the simulated inundation patterns with the well-documented 2012 flood event. By combining geospatial analysis with hydraulic modelling, the study seeks to generate practical evidence for flood-risk monitoring, hazard communication, and strategic mitigation planning in one of Nigeria′s most environmentally and socioeconomically important river basins.

Methodology

Study Area Description

Kogi State bridges two major Nigerian geological provinces: the Precambrian Basement Complex in the western and central parts, and the Cretaceous to Recent sedimentary formations associated with the Anambra and Benue Basins in the eastern and riverine lowlands near the Niger–Benue confluence (Nigerian Geological Survey Agency, 2010; Offodile, 2002). The Basement Complex is predominantly composed of migmatite–gneiss, schist belts, and older granites, with occurrences of charnockites and gabbroic intrusions. Mineralization, including gold, iron, and cassiterite, is commonly associated with these basement formations and structural features (Rahaman, 1988; Kogbe, 1989). In contrast, the sedimentary sequences consist mainly of sandstones, shales, and localized coal deposits, alongside extensive alluvial materials distributed along river valleys and floodplains (Kogbe, 1989).

The hydrological data utilized in this study were obtained from the gauging station located along the Lower Niger River in Lokoja, positioned at Latitude 07°52′12.69″N & Longitude 06°46′29.75″E, at theonfluence of the Niger and Benue Rivers (Nigeria Hydrological Services Agency, 2020).

Data Collection

A variety of current and past years′ data were gathered, analyzed, and collated in order to create the flood modeling and simulation. The Lower Niger River floodplain′s hydrological and hydraulic conditions are evaluated using these data as the foundation for further research and interpretation of the model′s findings.

In this study, NASA web imagery was used to provide accurate terrain and surface information required for hydraulic modelling. The NASA imagery specifically served as the primary source for extracting river geometry, including channel alignment, floodplain extent, & elevation characteristics. The Digital Elevation Model from NASA provided topographical data based on elevation that affect water flow and flood behaviour.

Furthermore, the imagery enabled the identification of key physical features such as riverbanks, surrounding landforms, and low-lying areas susceptible to flooding. These features were processed and geo-referenced within QGIS before being integrated into the HEC-RAS environment through RAS Mapper.

According to model requirements, the significant data include water level, discharge and various web imagery data. All collected data are summarized in the Table 1.

Discharge & Water Level Data

The Flow and Stage-hydrographs of Lower Niger River were extracted from the Lokoja gauge station of Nigeria Hydrological Services Agency yearbook for the year

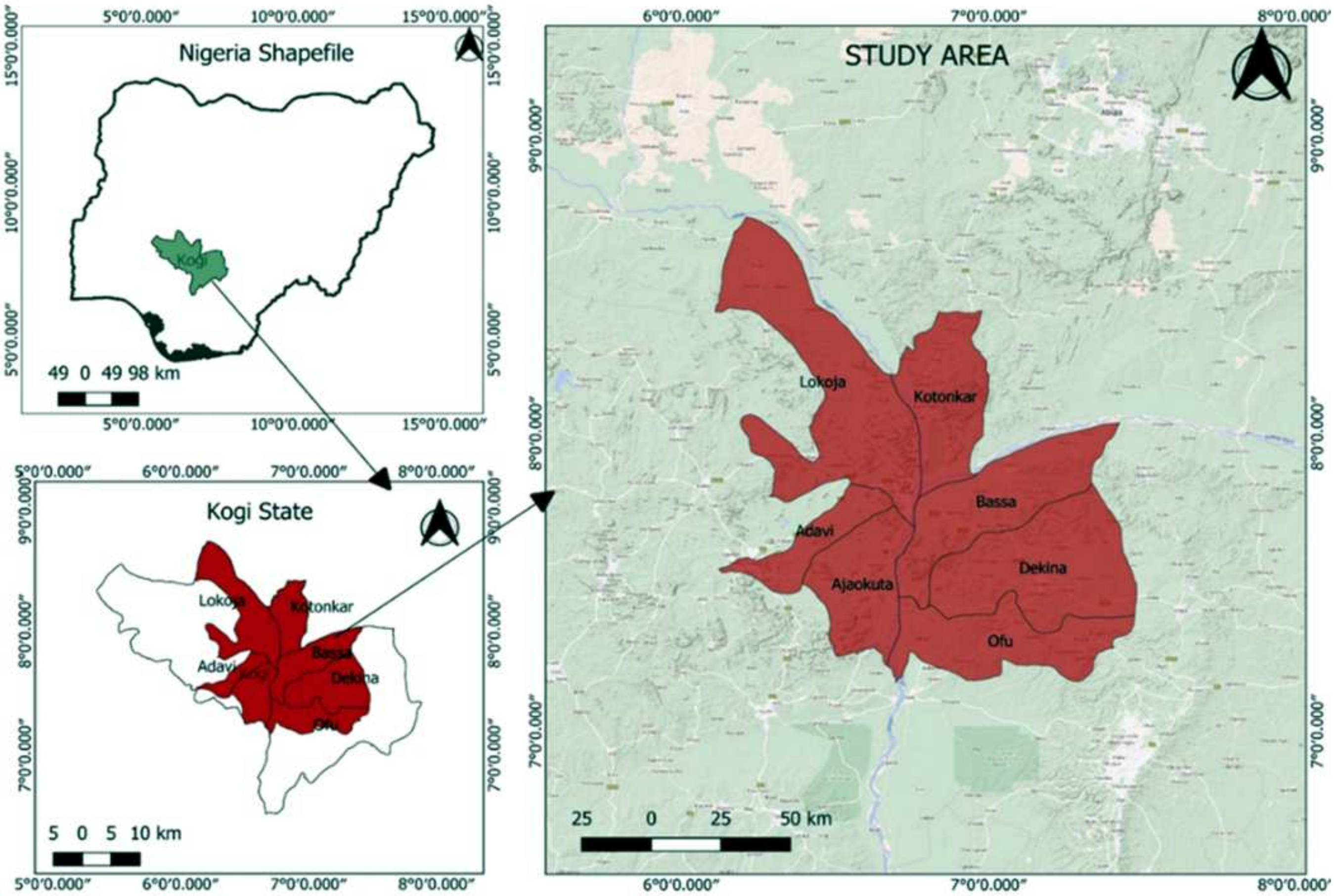

Fig. 1: Map showing the study area

Table 1: Summary of data type

Data Type	Data Source	Periods (year)
Discharge data	Nigeria Hydrological Services Agency	1995-2020
Water level	Nigeria Hydrological Services Agency	1995-2020
River Cross section	NASA Web Imagery	2023
Study Area DEM	United States Geological Survey (USGS)	2023
Satellite Image	(USGS)/ Earth Explorer	2023
Administrative map of study area	DIVA-GIS	2023
Land Use & Land Cover map layer	Esri - Sentinel-2 Land Cover Explorer	2017-2022

1995-2020 of the Federal Ministry of Water Resources. The Maximum annual discharge was used as Upper Limit boundary condition for the HEC-RAS simulation while the water level data was used as downstream boundary condition for the simulation. Table 2 shows Maximum Annual Discharge & Water Level (NIHSA, 2023).

Quantum Geographic Information System (QGIS)

QGIS is a cross-platform desktop geographic information system (GIS) application that supports viewing, editing, printing, & analysis of geospatial data. This software was used for geo-referencing & for processing of web images utilized in the study.

Preprocessing in RAS MAPPER

Geospatial preprocessing and hydraulic model development were carried out using RAS Mapper within the HEC-RAS environment, where geo-referenced datasets were processed to generate model-ready inputs from the Digital Terrain Model and associated spatial data (Figure 2). The river geometry was established by digitizing the river centerline, which defines the flow direction and extent of the model

Table 2: Water quality assessment result

S/N	Year	Max Annual Discharge	Max Annual Water Level
1	1995	17713	8.8
2	1996	19914	9.4
3	1997	15548	8.2
4	1998	23491	10.5
5	1999	23090	10.4
6	2000	18225	8.9
7	2001	18885	9.1
8	2002	17012	8.6
9	2003	19025	9.2
10	2004	16098	8.4
11	2005	13792	7.7
12	2006	19389	9.3
13	2007	19941	9.4
14	2008	20426	9.6
15	2009	20534	9.6
16	2010	21272	9.8
17	2011	17139	8.7
18	2012	31692	12.8
19	2013	16430	8.5
20	2014	19728	9.4
21	2015	27091	11.6
22	2016	20613	9.7
23	2017	21020	9.8
24	2018	25612	11.2
25	2019	24800	11.0
26	2020	28082	11.9

domain, extending from upstream to downstream along the Lower Niger River (Figure 3). Bank lines were traced to the left and right of the main channel to distinguish it from the floodplain, which enabled hydraulic properties such as Manning's n values to be applied differently to each area (Figure 4). Flow paths were delineated to allow flow routing to take place along the left overbank, the main channel and right overbank. The delineation of flow paths enables the downstream reach length to be calculated correctly by the model (Figure 5). Cross-sections were created orthogonal to the flow paths. Cross-sections are used as inputs into the hydraulic model and allow terrain elevations to be modelled from one side of the channel to the other across the floodplain (Figure 6). Cross-sections cut through the centreline, bank lines and flow paths allowing important hydraulic information such as bank stations, flow distances and geometry of the channel to be calculated. Manning's roughness coefficients were applied to each cross-section according to land cover. These values play a significant role in representing energy losses during flow and improving the realism of the simulation. Collectively, these processes ensured accurate representation of river geometry and floodplain characteristics, forming a reliable basis for subsequent flood modelling and analysis.

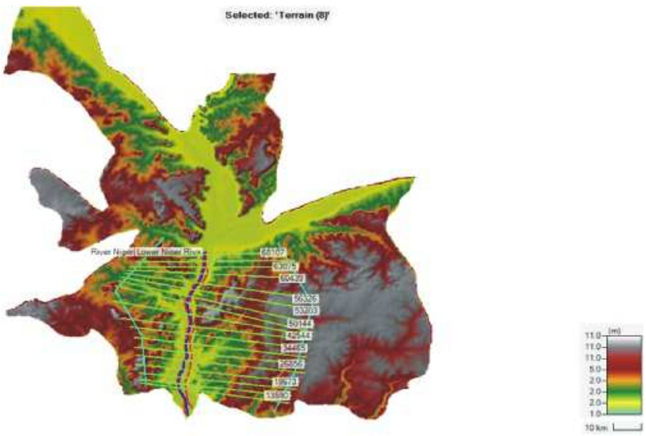

Fig. 2: RAS Mapper geometry processing

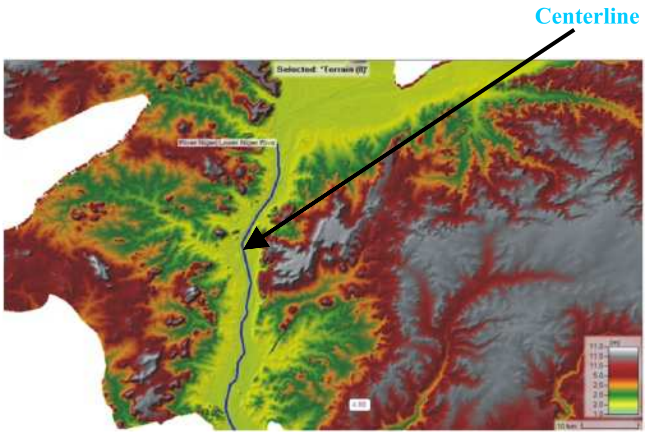

Fig. 3: Lower Niger River Centerline

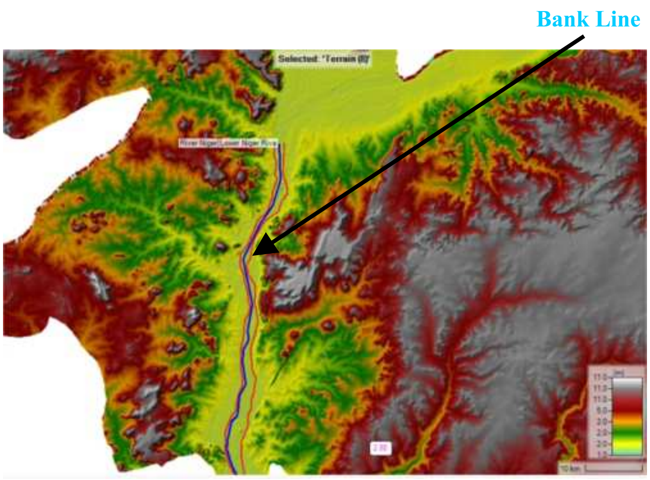

Fig. 4: Bank Line

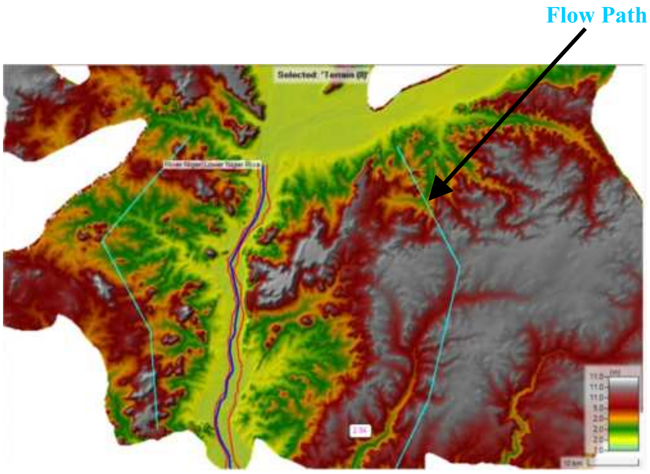

Fig. 5: Flow Path

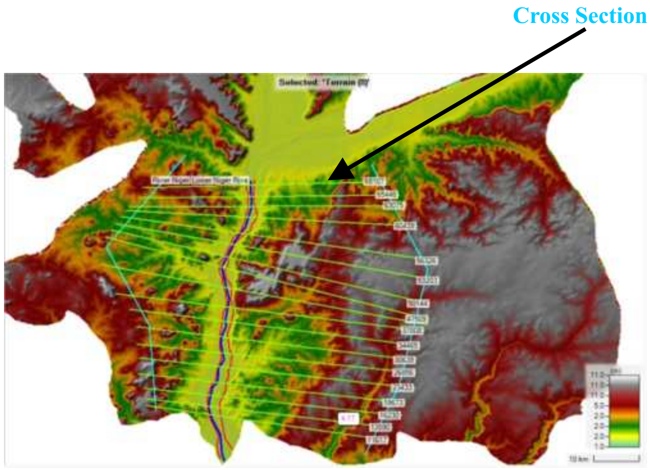

Fig. 6: Cross Section

Edit Manning's n or k Values

River: River Niger — Edit Interpolated XS's — Channel n Values have a light green background

Reach: Lower Niger Riva — All Regions

Selected Area Edit Options: Add Constant ... | Multiply Factor ... | Set Values ... | Replace ... | Reduce to L Ch R ...

	River Station	Frctn (n/K)	n #1	n #2	n #3
1	68107	n	0.07	0.035	0.07
2	65446	n	0.07	0.035	0.07
3	63075	n	0.07	0.035	0.07
4	60439	n	0.07	0.035	0.07
5	56326	n	0.07	0.035	0.07
6	53203	n	0.07	0.035	0.07
7	50144	n	0.07	0.035	0.07
8	47509	n	0.07	0.035	0.07
9	42544	n	0.07	0.035	0.07
10	37808	n	0.07	0.035	0.07
11	34465	n	0.07	0.035	0.06
12	30639	n	0.06	0.035	0.06
13	26856	n	0.06	0.035	0.06
14	23433	n	0.06	0.035	0.06
15	19673	n	0.06	0.035	0.06
16	16230	n	0.06	0.035	0.06
17	13590	n	0.06	0.035	0.06
18	11617	n	0.06	0.035	0.06

Fig. 7: Manning's 'n' values template

The Unsteady Flow Analysis

The Unsteady Flow Analysis window in HEC-RAS is a key component where simulations are performed and the analyses related to unsteady flow conditions in rivers and channels. Unsteady flow refers to situations where water flow varies with time, and it's essential for modeling events like floods or rapidly changing river conditions. For this research, unsteady flow analysis was carried out to simulate the various discharge readings from April, 2010 to March, 2020.

Calibration of HEC-RAS Model

The HEC-RAS model was calibrated referencing the September, 2012 flood stage (m) at Lokoja gaging station of 12.8m (NIHSA, 2023**;** Emmanuel *et al*, 2015). From the figure below, the water level from the simulation is 12.59m which falls within range to confirm the authentication of the model and the simulation.

Return Periods Calculation

For flood prediction of the case study, Gumbel′ Extreme value distribution method was utilized to obtain the flood return periods of 5, 10, 20, 30, 50, 100, 200 and 300years. Gumbel (1941) proposed this extreme value distribution, which is frequently referred to as Gumbel′s distribution. In hydrologic and meteorological research, it is one of the most often used probability functions for extreme values to forecast flood peaks, maximum

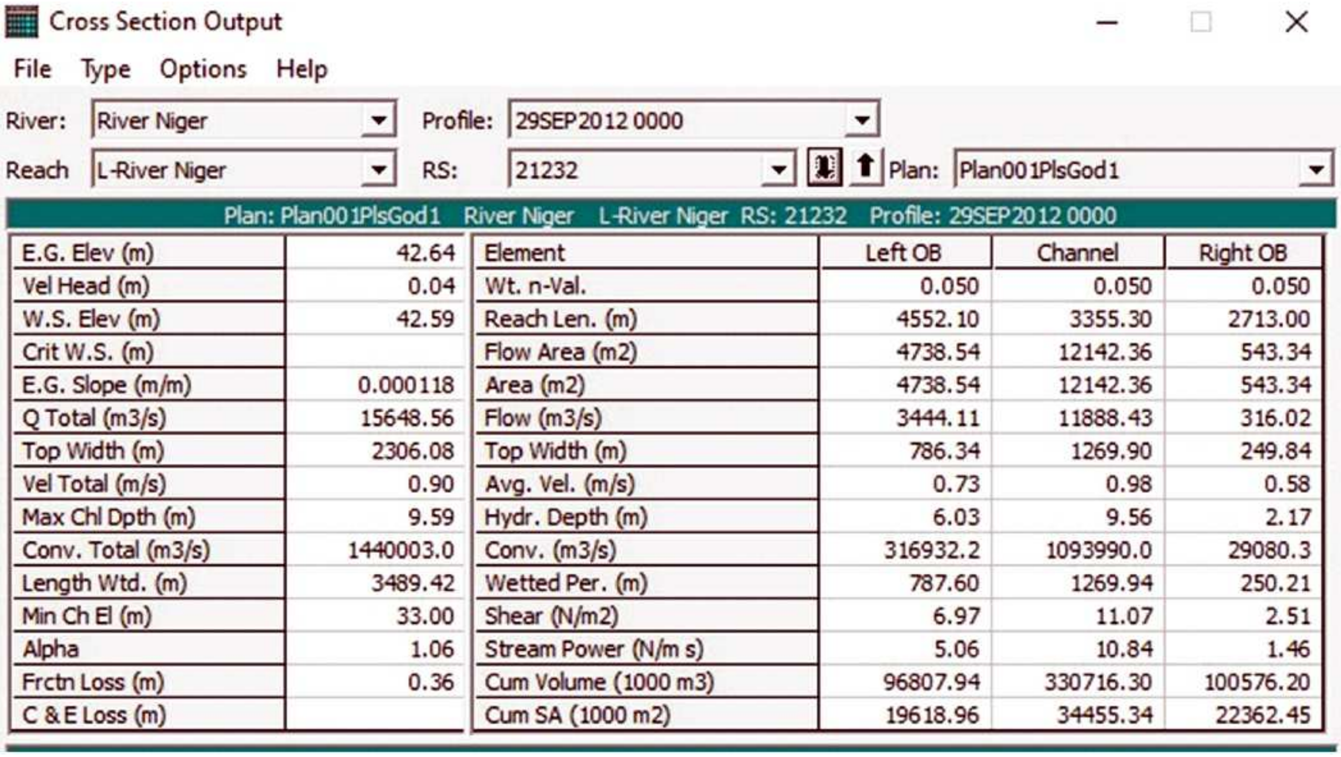

		Element	Left OB	Channel	Right OB
E.G. Elev (m)	42.64	Wt. n-Val.	0.050	0.050	0.050
Vel Head (m)	0.04	Reach Len. (m)	4552.10	3355.30	2713.00
W.S. Elev (m)	42.59	Flow Area (m2)	4738.54	12142.36	543.34
Crit W.S. (m)		Area (m2)	4738.54	12142.36	543.34
E.G. Slope (m/m)	0.000118	Flow (m3/s)	3444.11	11888.43	316.02
Q Total (m3/s)	15648.56	Top Width (m)	786.34	1269.90	249.84
Top Width (m)	2306.08	Avg. Vel. (m/s)	0.73	0.98	0.58
Vel Total (m/s)	0.90	Hydr. Depth (m)	6.03	9.56	2.17
Max Chl Dpth (m)	9.59	Conv. (m3/s)	316932.2	1093990.0	29080.3
Conv. Total (m3/s)	1440003.0	Wetted Per. (m)	787.60	1269.94	250.21
Length Wtd. (m)	3489.42	Shear (N/m2)	6.97	11.07	2.51
Min Ch El (m)	33.00	Stream Power (N/m s)	5.06	10.84	1.46
Alpha	1.06	Cum Volume (1000 m3)	96807.94	330716.30	100576.20
Frctn Loss (m)	0.36	Cum SA (1000 m2)	19618.96	34455.34	22362.45
C & E Loss (m)					

Fig. 8: Calibration of the model (water surface elevation of 42.59): (Note: the Datum height is 30m and the water level is 12.59m)

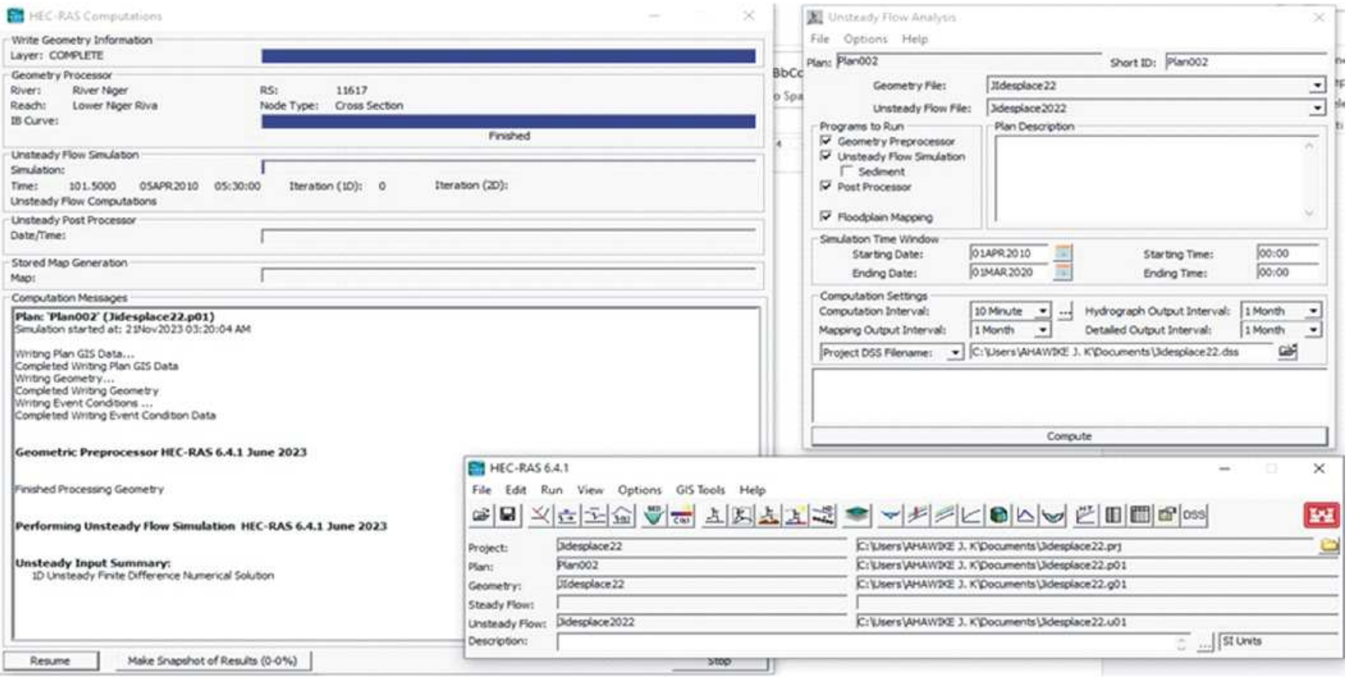

Fig. 9: Unsteady Flow Analysis

rainfall, maximum wind speed, etc. The following represents the Gumbel′s Distribution equation with return time T:

$$X_T=\bar{X}+K\times\sigma_x \quad \text{...(1)}$$

Where,

σ_x = Standard Deviation

K is Frequency Factor which is expressed as:

$$K=\frac{Y_t-\bar{Y}_n}{S_n} \quad \text{...(2)}$$

Y_t is reduced variate:

$$Y_t = -\left[In.In\left(\frac{T}{T\text{-}1}\right)\right] \text{...(3)}$$

Y_n and S_n are selected from Gumbel′s extreme volume distribution table considered depending on the sample size (n).

In order to estimate the design flood for different return periods, the following steps are adopted:

Step I: the annual peak flood is found in the daily data for a period of time.

Table 3: Maximum Annual Discharge and Water Level

S/N	Year	Max Annual Discharge(m^3/s)	Max Annual Water Level (m)
1	1995	17713	8.8
2	1996	19914	9.4
3	1997	15548	8.2
4	1998	23491	10.5
5	1999	23090	10.4
6	2000	18225	8.9
7	2001	18885	9.1
8	2002	17012	8.6
9	2003	19025	9.2
10	2004	16098	8.4
11	2005	13792	7.7
12	2006	19389	9.3
13	2007	19941	9.4
14	2008	20426	9.6
15	2009	20534	9.6
16	2010	21272	9.8
17	2011	17139	8.7
18	2012	31692	12.8
19	2013	16430	8.5
20	2014	19728	9.4
21	2015	27091	11.6
22	2016	20613	9.7
23	2017	21020	9.8
24	2018	25612	11.2
25	2019	24800	11.0
26	2020	28082	11.9

Step II: from series of annual maximum flood (step I) for n years the mean X_T & σ_x are computed using:

$$\bar{x} = \frac{1}{n}\sum_{i=1}^{n} x_i \text{...(4)}$$

$$\sigma_x = \sqrt{\left[\frac{1}{(n\text{-}1)}\sum_{i=1}^{n}(x_i\text{-}\bar{x})^2\right]} \text{.. (5)}$$

Step III: In the Gumbel′s extreme value distribution table, the $\bar{Y}_n$ & S_n values are obtained depending on sample size (n). The Gumbel′s extreme value distribution table is presented in Appendix II.

Step IV: from expected return period T_r, the reduced variant Y_t is computed using equation (3).

Step V: Flood frequency function K is computed using equation (2), given Y_n, S_n & Y_t.

Step VI: based on equation (1), the magnitude of flood is computed.

Before applying this method for flood frequency analysis one should first verify whether the input flood data series depicting the study area conforms to Gumbel′s distribution or not. The return period is assigned to each flood and the observed data is graded on descending scale (highest to lowest). By using equation (2), we compute the reduced variate corresponding to each flood. A graph of reduced variate & flood magnitude is plotted; if the plot yields a straight line, then we can safely assume that the observed flood data follows Gumbel′s distribution and is considered to fit well.

Table 4: Ranked Maximum Annual Discharge and Water Level

Year	Max Annual Discharge (m^3/s)	Max Annual Water Level (m)	Rank
2012	31692	12.8	1
2020	28082	11.9	2
2015	27091	11.6	3
2018	25612	11.2	4
2019	24800	11.0	5
1998	23491	10.5	6
1999	23090	10.4	7
2010	21272	9.8	8
2017	21020	9.8	9
2016	20613	9.7	10
2009	20534	9.6	11
2008	20426	9.6	12
2007	19941	9.4	13
1996	19914	9.4	14
2014	19728	9.4	15
2006	19389	9.3	16
2003	19025	9.2	17
2001	18885	9.1	18
2000	18225	8.9	19
1995	17713	8.8	20
2011	17139	8.7	21
2002	17012	8.6	22
2013	16430	8.5	23
2004	16098	8.4	24
1997	15548	8.2	25
2005	13792	7.7	26

From the above, the Mean and Standard Deviation is calculated using equations 4 and 5 above.

$$\bar{x} = \frac{1}{n}\sum_{i=1}^{n} x_i = \frac{536562}{26} = 20637$$

$$\sigma_x = \sqrt{\left[\frac{1}{(n-1)}\sum_{i=1}^{n}\left(x_i-\bar{x}\right)^2\right]} = \sqrt{\frac{436000948}{25}} = 4176.127144$$

From the table of Reduced Mean & Reduced Standard Deviation in Gumbel's Extreme Value Distribution for n = 26;

$Y_n = 0.5320$
$S_n = 1.0961$

Table 5: Reduced Variate

T	Expected Water Level (m) $X_T = (\bar{x} + K\sigma_{n-1})$	Expected Flood (m^3/s) $X_T = (\bar{x} + K\sigma_{n-1})$
5	10.8	24325
10	11.6	27184
20	12.4	29926
30	12.7	31504
50	13.5	33476
100	14.3	36137
200	15.0	38787
300	15.5	40335

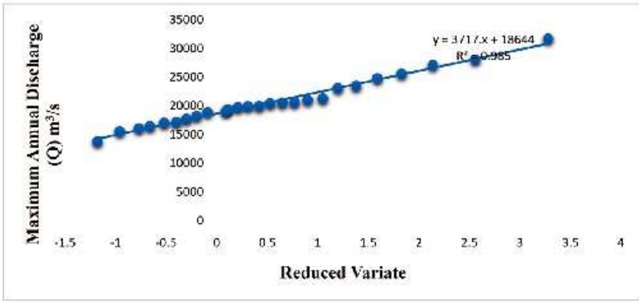

Fig. 10: Coefficient of Determination for Gumbel Extreme Distribution

The Figure 10 above with coefficient of determination/ R-square value (R^2)= 0.9856 indicates that Gumbel's extreme distribution is good fit for input flood data series. Therefore, adoption of Gumbel's Distribution for the determination of the various return periods for flood prediction at the Lower River Niger areas is satisfactory.

Results

Simulation

After all the necessary inputs were made in HEC-RAS, the simulation was run on the RAS Mapper to visualize the physical extend of the flood within study area.

Geometric Results from the HEC-RAS simulation

Discussion of Results

The results from the simulation show a steady and

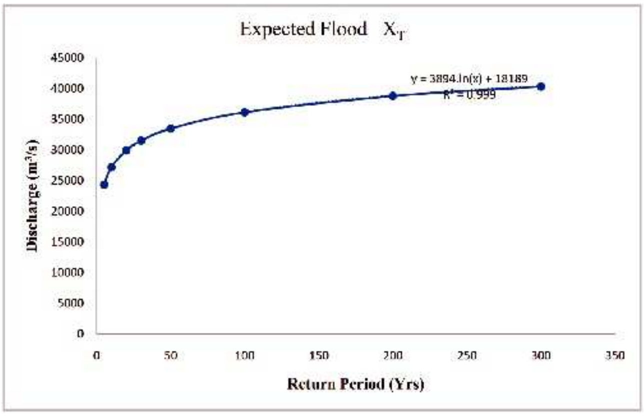

Fig. 11: Expected Discharge for the Return Periods

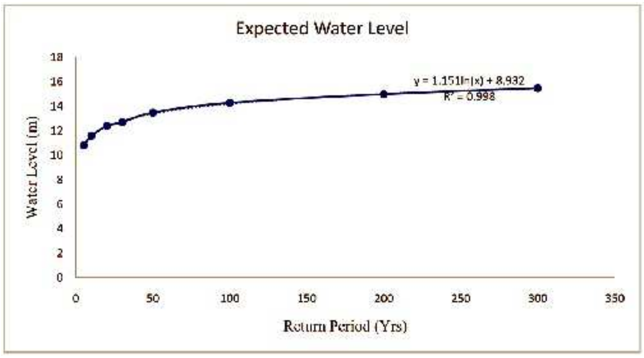

Fig. 12: Expected Water Level Return Periods

noticeable increase in flood extent as the return period becomes higher. This pattern can largely be explained by the physical characteristics of the Lower Niger River system. The study area is located at the confluence of the Niger and Benue Rivers, where the river channel tends to widen, the slope becomes gentler, and sediments are deposited over time. These conditions reduce the ability of the channel to confine flow, especially during periods of high discharge, causing water to spill over the banks and spread across the floodplain. As a result, the extent of flooding increases significantly with rising discharge levels.

Further analysis indicates that the flood extents associated with the 100-year and 300-year return periods are considerably larger than that recorded during the 2012 flood event. This increase is not only due to higher discharge values, reaching up to about 27% above the 2012 level, but also reflects reduced channel capacity caused by sediment build-up and increasing human activities within the floodplain. Similar behaviour has been observed in other low-gradient alluvial river systems, where floodwaters tend to spread widely under extreme flow conditions.

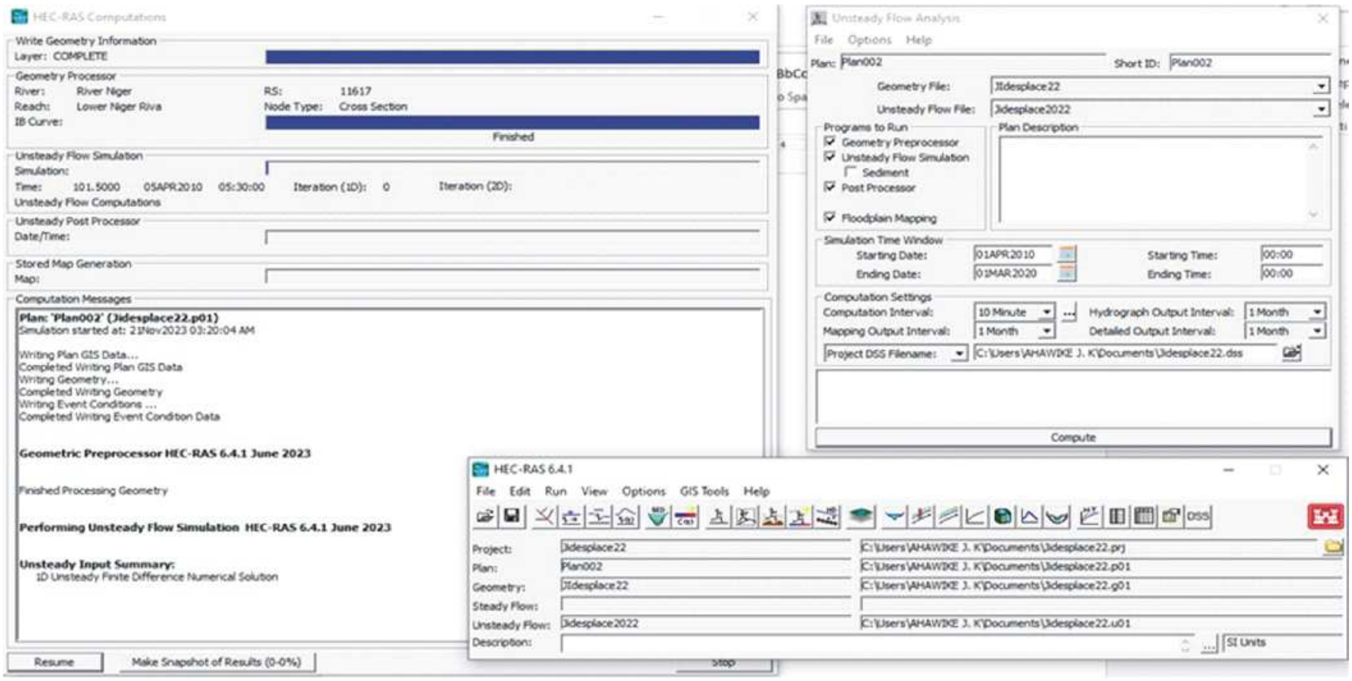

Fig. 13: Result for 30yr Return Period with a Water Level of 13.59m

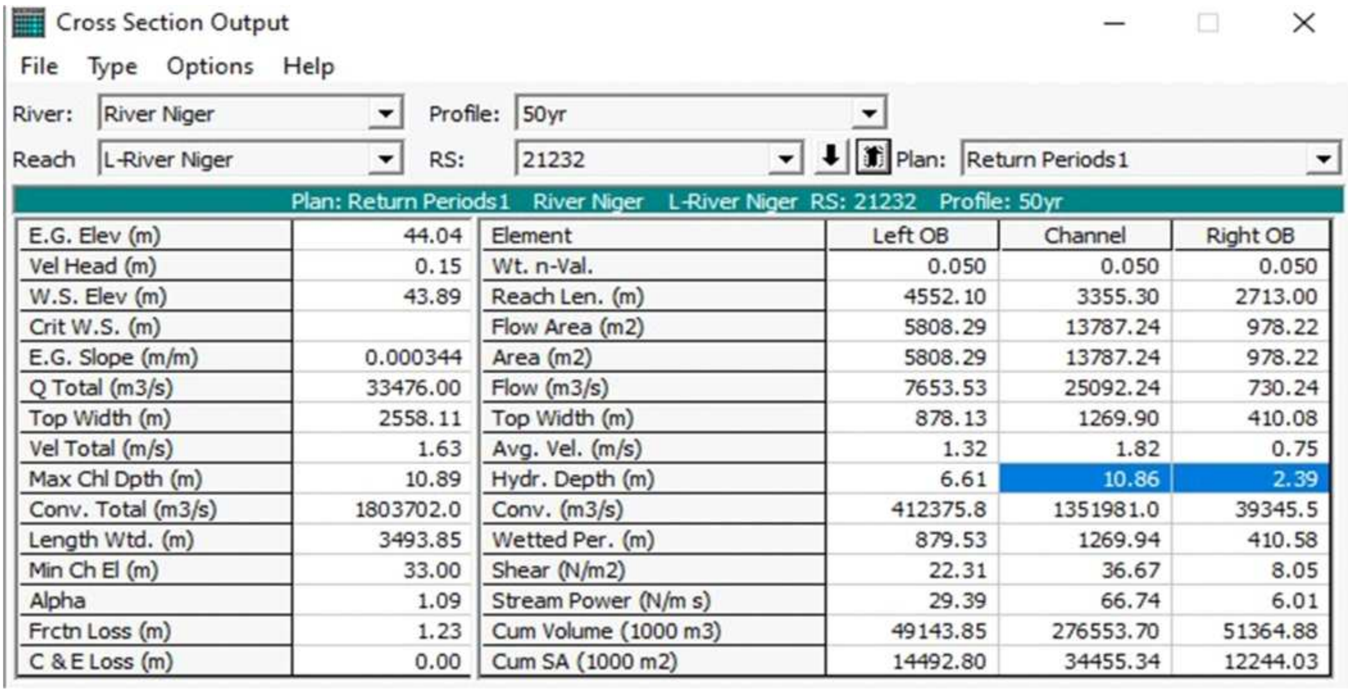

		Element	Left OB	Channel	Right OB
E.G. Elev (m)	44.04	Wt. n-Val.	0.050	0.050	0.050
Vel Head (m)	0.15	Reach Len. (m)	4552.10	3355.30	2713.00
W.S. Elev (m)	43.89	Flow Area (m2)	5808.29	13787.24	978.22
Crit W.S. (m)		Area (m2)	5808.29	13787.24	978.22
E.G. Slope (m/m)	0.000344	Flow (m3/s)	7653.53	25092.24	730.24
Q Total (m3/s)	33476.00	Top Width (m)	878.13	1269.90	410.08
Top Width (m)	2558.11	Avg. Vel. (m/s)	1.32	1.82	0.75
Vel Total (m/s)	1.63	Hydr. Depth (m)	6.61	10.86	2.39
Max Chl Dpth (m)	10.89	Conv. (m3/s)	412375.8	1351981.0	39345.5
Conv. Total (m3/s)	1803702.0	Wetted Per. (m)	879.53	1269.94	410.58
Length Wtd. (m)	3493.85	Shear (N/m2)	22.31	36.67	8.05
Min Ch El (m)	33.00	Stream Power (N/m s)	29.39	66.74	6.01
Alpha	1.09	Cum Volume (1000 m3)	49143.85	276553.70	51364.88
Frctn Loss (m)	1.23	Cum SA (1000 m2)	14492.80	34455.34	12244.03
C & E Loss (m)	0.00				

Fig. 14: Result for 50yr Return Period with a Water Level of 13.89m

From a geotechnical standpoint, the increasing intensity of flooding poses serious concerns for soil behaviour and infrastructure stability. Extended periods of flooding lead to soil saturation, which reduces shear strength and makes riverbanks more prone to erosion and possible collapse. In clayey soils, this may lead to a loss of load-bearing capacity, while in sandy soils, issues such as seepage and piping may develop. These conditions can weaken foundations and damage roads and embankments within affected areas.

The widening of flood-prone zones also raises important concerns for urban planning and infrastructure development. Many settlements and key

Cross Section Output

File Type Options Help

River: River Niger | Profile: 100yr

Reach: L-River Niger | RS: 21232 | Plan: Return Periods1

Plan: Return Periods1 River Niger L-River Niger RS: 21232 Profile: 100yr

		Element	Left OB	Channel	Right OB
E.G. Elev (m)	44.45	Element	Left OB	Channel	Right OB
Vel Head (m)	0.16	Wt. n-Val.	0.050	0.050	0.050
W.S. Elev (m)	44.29	Reach Len. (m)	4552.10	3355.30	2713.00
Crit W.S. (m)		Flow Area (m2)	6162.36	14294.15	1146.94
E.G. Slope (m/m)	0.000351	Area (m2)	6162.36	14294.15	1146.94
Q Total (m3/s)	36137.00	Flow (m3/s)	8412.65	26898.99	825.36
Top Width (m)	2596.22	Top Width (m)	895.94	1269.90	430.38
Vel Total (m/s)	1.67	Avg. Vel. (m/s)	1.37	1.88	0.72
Max Chl Dpth (m)	11.29	Hydr. Depth (m)	6.88	11.26	2.66
Conv. Total (m3/s)	1928952.0	Conv. (m3/s)	449057.7	1435838.0	44057.0
Length Wtd. (m)	3494.23	Wetted Per. (m)	897.38	1269.94	430.89
Min Ch El (m)	33.00	Shear (N/m2)	23.63	38.74	9.16
Alpha	1.10	Stream Power (N/m s)	32.26	72.90	6.59
Frctn Loss (m)	1.26	Cum Volume (1000 m3)	53679.16	287465.00	55251.88
C & E Loss (m)	0.00	Cum SA (1000 m2)	15125.04	34455.34	12951.63

Fig. 15: Result for 100yr Return Period with a Water Level of 14.29m

Cross Section Output

File Type Options Help

River: River Niger | Profile: 200yr

Reach: L-River Niger | RS: 21232 | Plan: Return Periods1

Plan: Return Periods1 River Niger L-River Niger RS: 21232 Profile: 200yr

E.G. Elev (m)	44.82	Element	Left OB	Channel	Right OB
Vel Head (m)	0.17	Wt. n-Val.	0.050	0.050	0.050
W.S. Elev (m)	44.66	Reach Len. (m)	4552.10	3355.30	2713.00
Crit W.S. (m)		Flow Area (m2)	6496.69	14763.70	1308.40
E.G. Slope (m/m)	0.000357	Area (m2)	6496.69	14763.70	1308.40
Q Total (m3/s)	38787.00	Flow (m3/s)	9150.04	28620.27	1016.69
Top Width (m)	2625.30	Top Width (m)	912.44	1269.90	442.96
Vel Total (m/s)	1.72	Avg. Vel. (m/s)	1.41	1.94	0.78
Max Chl Dpth (m)	11.66	Hydr. Depth (m)	7.12	11.63	2.95
Conv. Total (m3/s)	2053585.0	Conv. (m3/s)	484450.7	1515305.0	53828.8
Length Wtd. (m)	3496.56	Wetted Per. (m)	913.92	1269.94	443.48
Min Ch El (m)	33.00	Shear (N/m2)	24.87	40.67	10.32
Alpha	1.10	Stream Power (N/m s)	35.02	78.84	8.02
Frctn Loss (m)	1.28	Cum Volume (1000 m3)	58132.12	297749.80	59126.50
C & E Loss (m)	0.00	Cum SA (1000 m2)	15856.85	34455.34	13685.40

Fig. 16: Result for 200yr return period with a Water Level of 14.66m

facilities located in low-lying areas are becoming increasingly exposed to flood risks. If development in these areas continues without proper control, the level of vulnerability will only increase. The findings therefore emphasize the need for effective floodplain regulation, the integration of flood risk data into planning processes, and the design of infrastructure that can withstand extreme flood conditions.

Conclusion

This study has shown that integrating QGIS and HEC-RAS provides a reliable and practical framework for predicting floods and mapping hazard zones in the

Cross Section Output

File Type Options Help

River: River Niger Profile: 300yr

Reach L-River Niger RS: 21232 Plan: Return Periods1

Plan: Return Periods1 River Niger L-River Niger RS: 21232 Profile: 300yr

E.G. Elev (m)	45.04
Vel Head (m)	0.17
W.S. Elev (m)	44.86
Crit W.S. (m)	
E.G. Slope (m/m)	0.000360
Q Total (m3/s)	40335.00
Top Width (m)	2641.53
Vel Total (m/s)	1.75
Max Chl Dpth (m)	11.86
Conv. Total (m3/s)	2124884.0
Length Wtd. (m)	3497.78
Min Ch El (m)	33.00
Alpha	1.10
Frctn Loss (m)	1.30
C & E Loss (m)	0.00

Element	Left OB	Channel	Right OB
Wt. n-Val.	0.050	0.050	0.050
Reach Len. (m)	4552.10	3355.30	2713.00
Flow Area (m2)	6685.99	15025.84	1400.56
Area (m2)	6685.99	15025.84	1400.56
Flow (m3/s)	9582.32	29620.07	1132.61
Top Width (m)	921.65	1269.90	449.98
Avg. Vel. (m/s)	1.43	1.97	0.81
Hydr. Depth (m)	7.25	11.83	3.11
Conv. (m3/s)	504805.0	1560412.0	59667.0
Wetted Per. (m)	923.15	1269.94	450.50
Shear (N/m2)	25.59	41.81	10.99
Stream Power (N/m s)	36.68	82.42	8.88
Cum Volume (1000 m3)	60767.89	303562.40	61422.91
Cum SA (1000 m2)	16143.69	34455.34	14132.51

Fig. 17: Result for 300yr return period with a Water Level of 14.86m

Fig. 18: Google Satelite Imagery of the study area showing the normal water body and the surrounding environment before flooding.

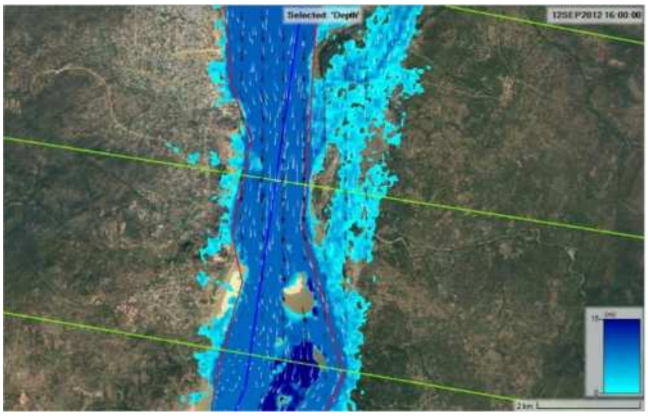

Fig. 19: Map Imagery of the study area showing simulated flood of Sepember 2012.

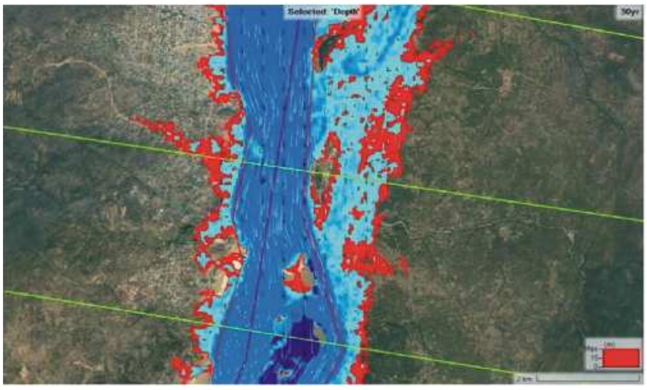

Fig. 20: Map Imagery of the study area showing simulated 30yr Return Period against the simulated 2012 flood.

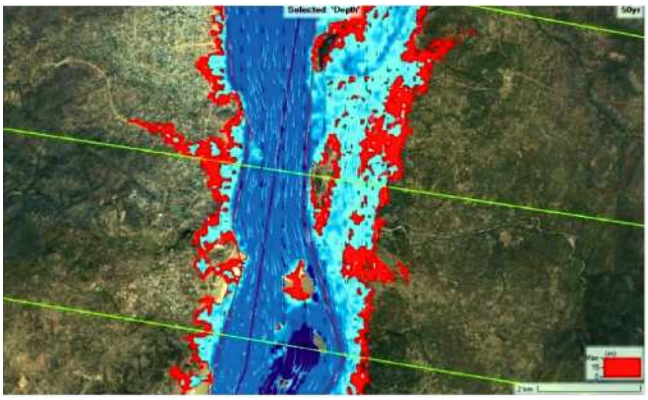

Fig. 21: Map Imagery of the study area showing simulated 50yr Return Period against the simulated 2012 flood.

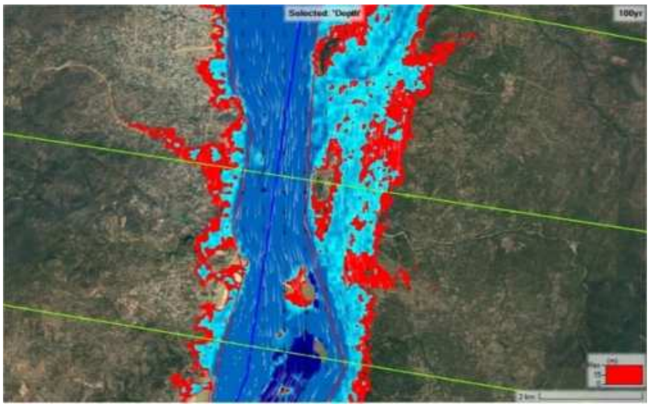

Fig. 22: Map Imagery of the study area showing simulated 100yr Return Period against the simulated 2012 flood.

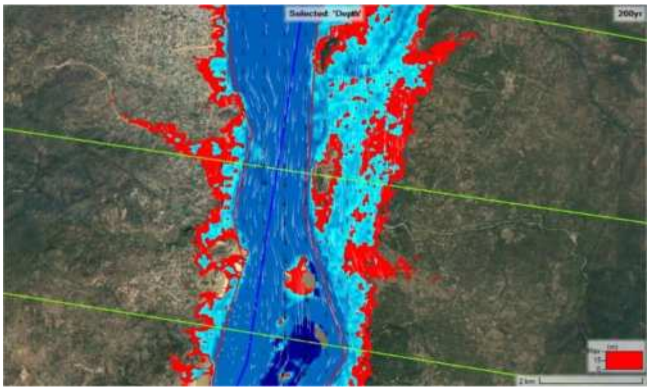

Fig. 23: Map Imagery of the study area showing simulated 200yr Return Period against the simulated 2012 flood.

Lower Niger Basin. The findings clearly indicate that both flood magnitude and spatial extent increase with return period. In particular, projected discharges exceed the 2012 flood by about 14% for the 100-year event and over 27% for the 300-year event, resulting in a significant expansion of inundated areas, especially within low-lying and morphologically sensitive zones.

The results further highlight the strong influence of river morphology on flood behaviour. Channel widening, sediment accumulation, and reduced flow velocity all contribute to limited flow confinement and increased

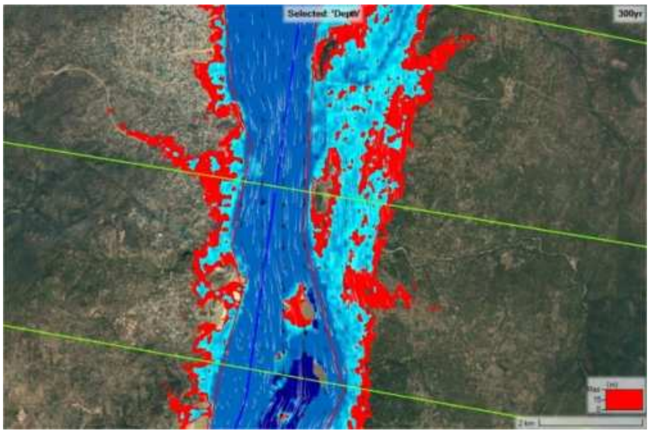

Fig. 24: Map Imagery of the study area showing simulated 300yr Return Period against simulated 2012 flood.

overbank flooding. Beyond hydrological impacts, repeated flooding has serious geotechnical consequences, including soil saturation, reduced shear strength, erosion, and loss of foundation stability. These conditions pose substantial risks to infrastructure such as roads, embankments, and buildings within the floodplain.

From an engineering and planning perspective, the study demonstrates that relying solely on historical flood records is no longer sufficient for effective risk assessment. Instead, predictive modelling should be fully integrated into infrastructure design, urban development, and floodplain regulation. The findings strongly support the need for targeted mitigation measures, including improved drainage systems, controlled land use, riverbank stabilization, and efficient early warning systems.

Overall, this study not only quantifies the growing flood risk in the Lower Niger region but also provides a clear, data-driven basis for action. Implementing such integrated modelling approaches is essential for reducing vulnerability, improving resilience, and supporting sustainable development in flood-prone areas.

References

Afzal M. A., Ali S., Nazeer, A., Khan M. I., Waqas M. M., Aslam R. A., Cheema M. J. M., Nadeem M., Saddique N. & Muzammil M. (2022). Flood Inundation Modeling by Integrating HEC–RAS and Satellite Imagery: A Case Study of the Indus River Basin. *Water*, 14, 2984. https:// doi.org/ 10.3390/w14192984

Bauer-Marschallinger B., Cao S., Tupas M. E., Roth F., Navacchi C., Melzer T., Freeman V., Wagner W. (2022). Satellite-Based Flood Mapping through Bayesian Inference from a Sentinel-1 SAR Datacube. *Remote Sensing.* 14 (3673). [Google Scholar] [CrossRef]

Chen Y. J., Lin H. J., Liou J. J., Cheng C. T., & Chen Y. M. (2022). Assessment of Flood Risk Map under Climate Change RCP8.5 Scenarios in Taiwan. *Water*, 14(2), 207. https:// doi.org/10. 3390/w14020207

Clare M. C. A., Piggott M. D. & Cotter C. J. (2022). Assessing erosion and flood risk in the coastal zone through the application of multilevel Monte Carlo methods. *Coastal Engineering Journal*. 174(104-118). [Google Scholar] [CrossRef]

Diao Y., Ma H., Wang H., Wang J., Li S., Li X., Pan J. & Qiu Q. (2022). Optimal Flood-Control Operation of Cascade Reservoirs Using an Improved Particle Swarm Optimization Algorithm. *Water*. 14(1239). [Google Scholar] [CrossRef]

Duchan D., Julínek T. & Říha J. (2022). Multicriterial analysis used for the optimisation of dike system management. *Journal of Flood Risk Management.* 15, e12829. [Google Scholar] [CrossRef]

Emmanuel U. A., Ojinnaka O. C., Baywood C. N., Gift U. A. (2015). Flood Hazard Analysis and Damage Assessment of 2012 Flood in Anambra State Using GIS and Remote Sensing Approach, *American Journal of Geographic Information System*, 4(1), pp. 38-51. doi:10.5923j.ajgis.201 50401.03..

Filipova V., Lawrence D. & Skaugen T. (2019). A stochastic event-based approach for flood estimation in catchments with mixed rainfall and snowmelt flood regimes. *Natural Hazards and Earth System Sciences. 19* (1–18). [Google Scholar] [CrossRef][Green Version

Gaisie E. & Cobbinah P. B. (2023). Planning for context-based climate adaptation: Flood management inquiry in Accra. *La Trobe. Journal contribution.* https://doi.org/10.26181/21913593.v1.

Gori A., Blessing R., Juan A., Brody S. & Bedient P. (2019). Characterizing urbanization impacts on floodplain through integrated land use, hydrologic, and hydraulic modeling. *Journal of Hydrologic Engineering.* 568(82–95). [Google Scholar] [CrossRef]

Grežo H., Močko M., Izsóff M., Vrbičanová G., Petrovič F., Straňák J., Muchová Z., Slámová M., Olah B., & Machar I. (2020). Flood Risk Assessment for the Long-Term Strategic Planning Considering the Placement of Industrial Parks in Slovakia. *Sustainability,* 12(10), 4144. https://doi.org/ 10.3390/su12104144.

Gumbel, E.J. (1941). The return period of flood flows. The Annals of Mathematical Statistics, 12, 163-190.

Hankin B., Metcalfe P., Beven K. & Chappell N. A. (2019). Integration of hillslope hydrology and 2D hydraulic modelling for natural flood management. *Hydrology Research.* 50 (1535–1548). [Google Scholar] [CrossRef][Green Version]

Herrera P.A., Marazuela M.A. & Hofmann T. (2022). Parameter estimation and uncertainty analysis in hydrological modeling. *WIREs Water*. 9 (e1569). [Google Scholar] [CrossRef]

IPCC 2021 Climate Change (2021). The Physical Science Basis. Contribution of Working Group I to the Sixth Assessment Report of the Intergovernmental Panel on Climate Change. Cambridge Univ. Press.

Kogbe, C.A., (1989). *The Cretaceous and Paleogene Sediments of Southern Nigeria. Geology of Nigeria 2nd Edition*. Rock View (Nig) Ltd, pp. 325-33.

Korah, P. I. & Cobbinah, P. B. (2019). Institutional Responses to Climate Change Adaptation: Flood Management at the Metropolitan Level in Accra, Ghana. In: Cobbinah, P.B., Addaney, M. (eds) The Geography of Climate Change Adaptation in Urban Africa. Palgrave Macmillan, Cham. https://doi.org/10.1007/ 978-3-030-04873-0_16.

Liu W. C., Hsieh T. H. & Liu H. M. (2021). Flood Risk Assessment in Urban Areas of Southern Taiwan. *Sustainability*, 13(6), 3180. https://doi.org/10.3390/su13063180.

Mondal K., Bandyopadhyay S. & Karmakar S. (2023). Framework for global sensitivity analysis in a complex 1D-2D coupled hydrodynamic model: Highlighting its importance on flood management over large data-scarce regions. *Journal of Environmental Management.* 332(117-312). [Google Scholar] [CrossRef]

Nharo, T., Makurira, H. & Gumindoga, W. (2019). Mapping floods in the middle Zambezi Basin using earth observation and hydrological modeling techniques. *Physical and Chemical Earth Science*. 114(1–9). https://doi.org /10.1016/ j.pce.2019. 06.002.

Nigeria Hydrological Services Agency (NIHSA). (2020). Hydrological Year Book. Federal Ministry of Water Resources, Abuja.

Nigerian Geological Survey Agency (NGSA). (2010). Geological Map of Nigeria. Abuja, Nigeria.

NIHSA (2023). Nigeria Hydrological Services Agency Flood Report. https://nihsa.gov.ng/

Nikoo M., Ramezani F., Hadzima-Nyarko M., Nyarko E. K. & Nikoo M. (2016). Flood-routing modeling with neural network optimized by social-based algorithm. *Natural Hazards.* 82 (1–24). [Google Scholar] [CrossRef]

Pinos J., Timbe, L. & Timbe E. (2019). Evaluation of 1D hydraulic models for the simulation of mountain fluvial floods: A case study of the Santa Bárbara River in Ecuador. *Water Practice & Technology.* 14(341–354). [Google Scholar] [CrossRef]

Psomiadis E., Tomanis L., Kavvadias A., Soulis K. X., Charizopoulos N. & Michas S. (2021). Potential Dam Breach Analysis and Flood Wave Risk Assessment Using HEC-RAS and Remote Sensing Data: A Multicriteria Approach. *Water*. 13, (364). [Google Scholar] [CrossRef]

Rahaman, M. A. (1988). *Recent Advances in the Study of the Basement Complex of Nigeria. In Precambrian Geology of Nigeria, Geological Survey of Nigeria, Kaduna South*, pp. 11-43.

Ramayanti, S., Nur, A. S., Syifa, M., Panahi, M., Achmad, A. R., Park, S. & Lee, C.-W. (2022). Performance comparison of two deep learning models for flood susceptibility map in Beira area, Mozambique. *The Egyptian Journal of Remote Sensing and Space Science*. 25(4). Pp 1025-1036, ISSN 1110-9823, https://doi.org/10.1016/j.ejrs.2022.11.003.

Rincón D., Khan U. T., & Armenakis C. (2018). Flood Risk Mapping Using GIS and Multi-Criteria Analysis: A Greater Toronto Area Case Study. *Geosciences*, 8(8), 275. https://doi.org/10.3390/geosciences8080275.

Santos P. P., Reis E., Pereira S., Santos M. (2019). A flood susceptibility model at the national scale based on multicriteria analysis. *Science of the Total Environment*. 667(325-337). doi: 10.1016/j.scitotenv.2019.02.328. Epub 2019 Feb 23. PMID: 30831369.

Schumann, G. J. P., Brakenridge, G. R., Kettner, A. J., Kashif, R. & Niebuhr, E. (2018). Assisting flood disaster response with earth observation data and products: a critical assessment. *Remote Sensing*. 10 (1–19). https://doi.org/10.3390/rs10081230.

Winter B., Schneeberger K., Dung N.V., Huttenlau M., Achleitner S., Stötter J., Merz B. & Vorogushyn S. (2019). A continuous modelling approach for design flood estimation on sub-daily time scale. *Hydrological Sciences Journal*. 64(539–554). [Google Scholar] [CrossRef][Green Version]

Wu J., Liu H., Wei G., Song T., Zhang C. & Zhou H. (2019). Flash flood forecasting using support vector regression model in a small mountainous catchment. *Water.* 11(1327). [Google Scholar] [CrossRef][Green Version].